Nanometer-scale sharpness in corner-overgrown heterostructures

L. Steinke,[1,a)] P. Cantwell,[2] D. Zakharov,[2] E. Stach,[2] N. J. Zaluzec,[3]
A. Fontcuberta i Morral,[1] M. Bichler,[1] G. Abstreiter,[1] and M. Grayson[1,4,b)]
[1]*Walter Schottky Institut, Technische Universität München, D-85748 Garching, Germany*
[2]*School of Materials Engineering, Purdue University, West Lafayette, Indiana 47907, USA*
[3]*Electron Microscopy Center, Materials Science Division, Argonne National Laboratory, Argonne, Illinois 60439, USA*
[4]*Department of Electrical Engineering and Computer Science, Northwestern University, Evanston, Illinois 60208, USA*

(Received 14 July 2008; accepted 18 August 2008; published online 14 November 2008)

A corner-overgrown GaAs/AlGaAs heterostructure is investigated with transmission and scanning transmission electron microscopy, demonstrating self-limiting growth of an extremely sharp corner profile 3.5 nm wide. In the AlGaAs layers, we observe self-ordered diagonal stripes, precipitating exactly at the corner, which show increased Al content measured with x-ray spectroscopy. A quantitative model for self-limited growth is adapted to the present case of faceted molecular beam epitaxial growth, and the corner sharpness is discussed in relation to quantum confined structures. We note that corner overgrowth maintains nanometer sharpness after microns of growth, allowing corner-shaped nanostructures. © *2008 American Institute of Physics*. [DOI: 10.1063/1.2988526]

The corner-overgrowth technique has been demonstrated previously[1] to create a 90° junction between high-mobility two-dimensional electron systems. In a magnetic field, this system realizes a unique sort of quantum Hall effect boundary state with either co- or counterpropagating edge modes at various filling factors.[2,3] In all cases, the sharpness of the confinement potential is essential to understanding the electronic structure of the device. In this letter, high-resolution transmission and scanning transmission electron microscopy (TEM/STEM) as well as simultaneous x-ray energy dispersive spectroscopy (XEDS) measurements on corner-overgrown heterostructures quantify the sharpness of the corner profile and give further insight into the growth mechanisms at such a corner junction.

A detailed description of the growth technique is found in Ref. 1. The samples were grown in an ultrahigh vacuum Epi GEN-II molecular beam epitaxy (MBE) system ($P < 10^{-9}$ Pa). GaAs (110) substrate pieces were cleaved *ex situ* to create atomically sharp corners between two orthogonal (110) and $(1\bar{1}0)$ facets and were mounted inside the MBE chamber, with the corner facing the molecular flux. After oxide desorption, the samples were overgrown under rotation ($d\alpha/dt = 5$ rpm) at a substrate temperature of $T_{sub} = 460$ °C and an As_4 pressure of 3.5×10^{-3} Pa. Figure 1 illustrates the layer sequence, which consists of 71 nm wide AlAs layers separated by $Al_{0.3}Ga_{0.7}As$/GaAs superlattices with the period (8.0 nm/2.3 nm). The AlAs layers were grown to obtain high contrast images of the corner structure in both scanning and transmission electron microscopes.

The specimen was prepared for TEM using a FEI xT Nova NanoLab dual beam focused ion beam (FIB)/scanning electron microscope. During FIB preparation, a variation of the liftout technique[4] was used to extract an approximately 1 μm thick cross section of the corner-overgrown heterostructure. The cross section was then attached to a copper TEM half-grid using platinum and was further thinned to ~100 nm. Microanalytical and high angle annular dark field (HAADF) STEM studies were conducted on a FEI Tecnai F20 TEM/STEM equipped with both XEDS and electron energy loss spectroscopy, which was operated at 200 kV. In addition, high-resolution TEM images were obtained using a FEI Titan 80/300 field emission TEM operating at 300 kV. Figure 1 presents a HAADF STEM image of the heterostructure, demonstrating regularly shaped corners and equal layer thicknesses on both overgrown facets.

We observe stripes of high contrast along the diagonal of the intersection between perpendicular AlGaAs layers in the structure. Figure 2 displays a HAADF STEM image of these diagonal stripes taken from region A in Fig. 1. The contrast in a HAADF image is dominated by atomic number effects, and higher average atomic number regions appear brighter

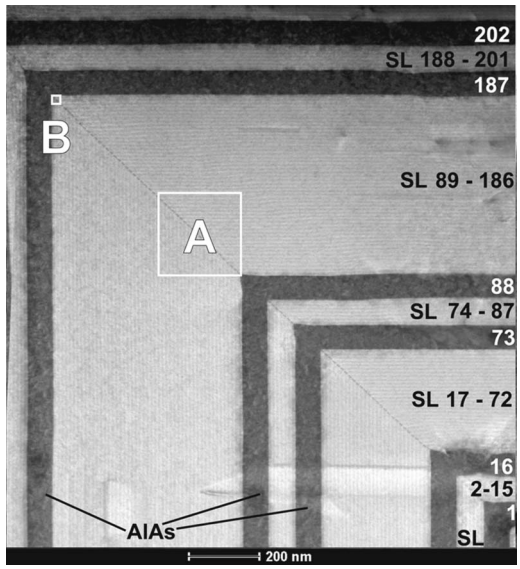

FIG. 1. HAADF STEM image of the heterostructure, demonstrating sharp corners and equal layer thicknesses on both overgrown facets. The grown layer sequence consists of 71 nm wide AlAs layers separated by GaAs/AlGaAs superlattices, where the numbers on the right count the layer index. The superlattice in region A is displayed at higer magnification in Fig. 2, and a high-resolution bright field image of region B is shown in Fig. 3.

a)Electronic mail: m-grayson@northwestern.edu.
b)Author to whom correspondence should be addressed. Electronic mail: m-grayson@northwestern.edu.

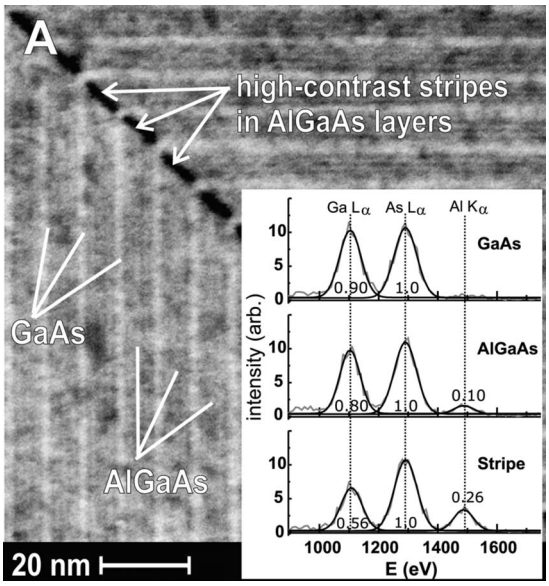

FIG. 2. HAADF STEM image of high contrast stripes along the diagonal of AlGaAs layers in the superlattice in region A of Fig. 1. The inset shows XEDS spectra from three different regions, using a ~1 nm probe: GaAs, AlGaAs, and one of the diagonal stripes. Numbers next to the peaks indicate the measured intensities, normalized to the As $L\alpha$ peak area.

due to their increased scattering cross section.[5] In addition, in Fig. 2 we observe a secondary substructure of weaker but clearly resolved alternating bright and dark stripes in the growth direction of the individual AlGaAs layers. This indicates periodic variations of the Al content as the tilted facets rotate under the asymmetrically placed Al and Ga beams.[1] The material composition of the regions of interest was investigated with XEDS in Fig. 2 (inset) at three different locations: GaAs, AlGaAs, and one of the diagonal stripes. Here the gray lines are the actual experimental data, while the black lines are Gaussian peak fits to determine the local compositions. All spectra were normalized to the As $L\alpha$ line since we expect an equal As concentration in the three measured regions. The Al content is estimated by a simple algebraic scaling of intensity ratios[6] from the stripe spectrum to the AlGaAs spectrum at a known average Al content of $x=0.301$. We obtain two independent estimates: $x^K=0.78$ from the Al $K\alpha$ intensities and $x^L=0.51$ from the Ga $L\alpha$ intensities. Using the mean value, we arrive at $\bar{x}=0.65\pm0.1$ in the diagonal stripes, a significant increase compared to the neighboring $Al_{0.3}Ga_{0.7}As$.

A high-resolution bright-field TEM image taken at the AlGaAs/AlAs interface between layers 186/187 (region B in Fig. 1), after 1.2 μm of growth, reveals a sharp corner profile with evidence of a flat top of 3.5 nm width, which appears to be parallel to the (100) facet (Fig. 3, top). The initial curvature of the overgrown corner, due to the oxidation of the *ex situ* cleaved substrate,[7] heals to this extremely sharp faceted profile. The effective radius of curvature r_{eff} ~5 nm at the corner is a useful parameter for estimating quantum confinement, defined here as the radius of the smallest circle tangent to the (110) and $(1\bar{1}0)$ side facets and the flat top region. The quarter-circle in Fig. 3 is shifted away from the interface to give a clear view of the corner profile.

Both a faceted corner profile and the observed adatom segregation in AlGaAs layers are predicted in an analytic model by Biasiol *et al.*,[8,9] explaining self-ordering of nanostructures grown on nonplanar surfaces. If the growth rates on the side facets (r_s) and the top facet (r_t) show an anisotropy such that $\Delta r=r_s-r_t<0$, the faster growth on the side facets leads to a narrowing of the top facet. This effect is compensated by an increasing capillarity flux of adatoms away from the top facet, caused by an increase of the chemical potential at the narrowing top facet. The ridge structure develops a self-limiting profile of width l_t^{sl}, which for binary compounds such as GaAs can be expressed by[8,9]

$$l_t^{\mathrm{sl}}=\left(\frac{2\Omega_0 L_s^2\gamma}{k_BT}\frac{r_s}{-\Delta r}\right)^{1/3}. \tag{1}$$

Here, Ω_0 is the atomic volume of 11.8 $\mathrm{cm}^3/\mathrm{mol}$ and L_s is the adatom diffusion length on the sidewall. The surface free energy term $\gamma=2(\gamma_s\csc\theta-\gamma_t\cos\theta)$ depends on the surface free energies of the top facet and the sidewall, γ_t and γ_s, and on the angle θ between the facets. The scenario for ternary alloy layers, such as the AlGaAs layer in Fig. 2, is more complicated: the different adatom diffusion lengths lead to different capillarity fluxes for the two adatom species, causing a region rich in the slow-diffusing species (Al) at the top facet. After Biasiol *et al.*,[9] the self-limiting width $l_{t,\mathrm{alloy}}^{\mathrm{sl}}$ is the solution to the equation

$$\frac{a}{(l_{t,\mathrm{alloy}}^{\mathrm{sl}})^3}+\frac{b}{(l_{t,\mathrm{alloy}}^{\mathrm{sl}})^2}=\Delta r(x), \tag{2}$$

with

$$a=x\Delta r_{\mathrm{Al}}(l_{t,\mathrm{Al}}^{\mathrm{sl}})^3+(1-x)\Delta r_{\mathrm{Ga}}(l_{t,\mathrm{Ga}}^{\mathrm{sl}})^3,$$

$$b=2\left\{x(L_{s,\mathrm{Al}})^2\ln(x/x_t)+(1-x)(L_{s,\mathrm{Ga}})^2\ln\left[\frac{1-x}{1-x_t}\right]\right\},$$

$$\Delta r(x)=x\Delta r_{\mathrm{Al}}+(1-x)\Delta r_{\mathrm{Ga}},$$

where the subscripts Ga and As refer to the parameters for pure GaAs and AlAs growths respectively. The logarithmic terms account for the entropy of mixing, with x as the Al content of the AlGaAs layer and x_t as the local Al content at the top facet.

To compare our experimental findings to the predictions of this analytical growth model, we calculate the self-limiting width expected for an $Al_{0.3}Ga_{0.7}As$ alloy layer from Eqs. (1) and (2). From Ref. 10 we estimate the surface free energies $\gamma_s\approx\gamma_t\approx45$ meV/Å^2 under As_4 rich growth conditions and obtain $\gamma=\sqrt{2}\gamma_s$ for the surface free energy term at $\theta=45°$. Experimental values for the Ga diffusion length on the (110) facet are found in Refs. 11 and 12. Extrapolating the temperature dependence measured by López *et al.*[11] at an As_4 pressure of 1.2×10^{-3} Pa, we obtain $L_s\approx40$ nm at our growth temperature of 460 °C. The diffusive growth rate anisotropy Δr_{Ga} is estimated as well from experimental results in Ref. 11, showing a reduced growth rate on (110) facets. We find a ratio of 1/0.23 between (100) and (110) growth rates at our growth conditions. In addition, the growth rate at the edges of a (100) top facet is found to be locally enhanced by an additional adatom flux from the (110) side facets. We extrapolate from the side wall distance an additional growth rate enhancement of 45% for a very narrow (100) top facet. For GaAs we therefore obtain a factor $r_{s,\mathrm{Ga}}/-\Delta r_{\mathrm{Ga}}\approx1/(1.45/0.23-1)$. Lacking experimental values, we assume the same growth rate anisotropy for AlAs growth since the final result $l_{t,\mathrm{alloy}}^{\mathrm{sl}}$ is not very sensitive to this parameter.[13] With the Al diffusion length $L_{s,\mathrm{Al}}$ as the remain-

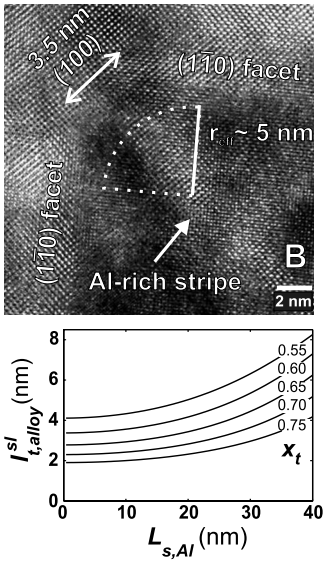

FIG. 3. Top panel shows a high-resolution bright-field TEM image of the interface between layers 186/187 (AlGaAs/AlAs) in sample region B marked in Fig. 1, at a total grown thickness of 1.2 μm. One of the Al-rich diagonal stripes in Fig. 2 appears as a bright stripe of 2 nm width. The interface to the AlAs layer 187 shows a sharp profile with a 3.5 nm wide (100) top facet. The bottom panel shows the self-limiting width calculated from Eq. (2) for an $Al_{0.3}Ga_{0.7}As$ alloy profile, as a function of the Al diffusion length $L_{s,Al}$ for various Al concentrations x_t in the diagonal stripes.

ing free parameter, we calculate the self-limiting width $l^{sl}_{t,alloy}$ of an $Al_{0.3}Ga_{0.7}As$ alloy layer for various values of the Al content x_t in the accumulation region. Figure 3 shows $l^{sl}_{t,alloy}$ as a function of the Al diffusion length in the limits $0 < L_{s,Al} < L_{s,Ga} = 40$ nm. For $L_{s,Al} \ll L_{s,Ga}$, the measured top facet width of 3.5 nm would correspond to an Al content of $x_t = 0.6$, which is well within the error bars of our XEDS result $x_t = 0.65 \pm 0.1$. At larger values of the Al diffusion length, the measured width would still be within the limits of variation of the measured Al content x_t. This shows that the growth model in Refs. 8 and 9 provides reasonable estimates of the Al segregation and the width of the self-limiting profiles created by MBE corner overgrowth.

The measured sharpness of the corner-overgrown layers also answers important questions about the electronic structure of bent quantum Hall junctions.[3] For example, a one-dimensional accumulation wire has been predicted to exist at $B=0$ in the structures of Ref. 3 if the diameter of curvature $2r$ is smaller than half the Fermi wavelength λ_F. For typical sheet electron densities between 1.0×10^{11} and 1.5×10^{11} cm^{-2}, λ_F is between 80 and 65 nm, so from our measurements the condition $2r < \lambda_F/2$ is satisfied, and a one-dimensional wire with a single occupied subband should exist at the corner. To calculate the electronic dispersions in the presence of a B-field, the comparison between the magnetic length l_B and the triangular confinement width W becomes relevant. The wavefunction full width at half maximum $W = 18$ nm is estimated from Hartree calculations of the triangular confinement for the above densities. For small magnetic fields such that $W/2 < l_B$ ($B < 8$ T), the $B=0$ Hartree potential can be safely used in place of the finite B Hartree potential, drastically simplifying the dispersion calculation as in Ref. 3. At larger magnetic fields such that $W/2 > l_B$ ($B < 8$ T), dispersion calculations should include the B-field in the Hartree iteration. Finally, at extreme fields the radius of curvature of the corner $r_{\text{eff}} = 5$ nm becomes important once $r > l_B$ ($B > 26$ T). At these high fields, the sharp corner approximation for the external potential should be replaced with a real potential with finite corner curvature. The corner-overgrown profiles measured here are sharp enough that one is able to achieve a fractional filling factor $\nu = 1/3$ for typical densities before reaching this limit.

In conclusion, the TEM/STEM/XEDS results demonstrate that corner-overgrowth yields extremely sharp self-limited corner profiles, justifying the assumption of a sharp corner potential in bent quantum Hall junctions.[3] Compared to the TEM images of self-ordered diagonal stripes in Ref. 9, the stripes observed in our corner-overgrown structure are a factor of 5 thinner. Both the width of the self-limited profile and the Al adatom segregation observed in XEDS measurements on the AlGaAs layers can be estimated from a quantitative growth model[8,9] with reasonable assumptions. Due to the self-limitation, it is possible to grow sharp corner profiles that persist over microns of growth, where the minimum width is determined by the growth conditions. This shows that MBE corner overgrowth allows the precise control of one-dimensional quantum confinement and justifies the assumptions of previous work of a sharp corner with a one-dimensional accumulation wire.[2,3]

This work was supported by the Deutsche Forschungsgemeinschaft (DFG) through contract No. GR 2618/1-1. Work was performed at the Electron Microscopy Center of Argonne National Laboratory, a U.S. Department of Energy Office of Science Laboratory operated under Contract No. DE-AC02-06CH11357 by UChicago Argonne, LLC.

[1] M. Grayson, D. Schuh, M. Huber, M. Bichler, and G. Abstreiter, Appl. Phys. Lett. **86**, 032101 (2005); D. Schuh, M. Grayson, M. Bichler, and G. Abstreiter, Physica E (Amsterdam) **23**, 293 (2004).
[2] M. Grayson, D. Schuh, M. Bichler, M. Huber, G. Abstreiter, L. Hoeppel, J. Smet, and K. v. Klitzing, Physica E (Amsterdam) **22**, 181 (2004).
[3] M. Grayson, L. Steinke, D. Schuh, L. Hoeppel, J. Smet, D. Maude, K. v. Klitzing, M. Bichler, and G. Abstreiter, Phys. Rev. B **76**, 201304(R) (2007).
[4] B. I. Prenitzer, L. A. Giannuzzi, K. Newman, S. R. Brown, R. B. Irwin, T. L. Shofner, and F. A. Stevie, Metall. Mater. Trans. A **29**, 2399 (1998).
[5] A. Crewe, J. Wall, and J. P. Langmore, Science **168**, 1138 (1970).
[6] N. J. Zaluzec, *Analytical Electron Microscopy*, edited by. R. H. Geiss (San Francisco, San Francisco, 1981), pp. 47–53; Ultramicroscopy **28**, 226–235 (1989).
[7] A high-resolution TEM image of the corner showed an initial radius of curvature $r \sim 12$ nm at the interface between the GaAs substrate and the first AlAs layer.
[8] G. Biasiol and E. Kapon, Phys. Rev. Lett. **81**, 2962 (1998); G. Biasiol, K. Leifer, and E. Kapon, Phys. Rev. B **61**, 7223 (2000).
[9] G. Biasiol, A. Gustafsson, K. Leifer, and E. Kapon, Phys. Rev. B **65**, 205306 (2002).
[10] N. Moll, A. Kley, E. Pehlke, and M. Scheffler, Phys. Rev. B **54**, 8844 (1996).
[11] M. López and Y. Nomura, J. Cryst. Growth **150**, 68 (1995); M. López, T. Ishikawa, and Y. Nomura, Jpn. J. Appl. Phys., Part 2 **32**, L1051 (1993).
[12] A. Yamashiki and T. Nishinaga, J. Cryst. Growth **198/199**, 1125 (1999).
[13] For example, at intermediate values $x_t = 0.65$ and $L_{s,Al} = 10$ nm, $l^{sl}_{t,alloy}$ varies only from 2.6 to 3.0 nm as the AlAs growth rate anisotropy is varied between −200 and −0.02.